11th International Symposium on Turbulence and Shear Flow Phenomena (TSFP11)
Southampton, UK, July 30 to August 2, 2019

TURBULENCE STRUCTURE IN NON-EQUILIBRIUM BOUNDARY LAYERS WITH FAVOURABLE AND ADVERSE PRESSURE GRADIENTS

Ralph J. Volino

Department of Mechanical Engineering
United States Naval Academy
590 Holloway Rd.
Annapolis, Maryland, 21012, USA
volino@usna.edu

ABSTRACT

An experimental study was conducted to document the turbulence in boundary layers on smooth walls subject to a favourable pressure gradient followed by a zero pressure gradient recovery and an adverse pressure gradient. Two component velocity profiles were acquired along the spanwise centreline of the test section, and velocity fields were obtained at the same locations in streamwise wall-normal and streamwise-spanwise planes using PIV. The FPG was shown to reduce the turbulence in the outer part of the boundary layer, reducing the transport of this turbulence and the effect of sweeps toward the wall. This reduced the inclination angle of the large structures and increased their length scale, particularly in the streamwise and spanwise directions. Recovery from the FPG to a ZPG was rapid. The APG reduced the near wall shear, resulting in a reduced effect of bursts relative to sweeps. The APG had an opposite but smaller effect on the shape and size of structures compared to the FPG.

INTRODUCTION

The presence of complex structures in turbulent boundary layers is well known. Some of the flow features extend for long distances in the streamwise direction and are known as large scale motions (LSM). The work of Adrian et al. (2000) and Hambleton et al. (2006) are two of several studies in which particle image velocimetry (PIV) was used to directly document instantaneous velocity fields and show the various structures. The LSM play a large role in determining boundary layer behavior. Ganapathisubramani et al. (2003), for example, noted that they contribute a large fraction of the total shear stress in a boundary layer.

The studies noted above and others have provided great insight into the nature of boundary layer flows and provided useful information for the development of improved turbulence models. Most have been done under zero pressure gradient (ZPG) conditions. While the ZPG case is the logical starting point for study and much has been learned from it, many flows of fundamental and practical interest include non-zero pressure gradients. Flows over aircraft and naval vessels and within turbomachinery, for example, include both favourable (FPG) and adverse (APG) pressure gradient regions. Typically the pressure gradient changes in the streamwise direction, so the boundary layer is not in equilibrium.

Fundamental studies of non-zero pressure gradient boundary layers include Aubertine and Eaton (2005), who considered a mild APG and noted differences in turbulence statistics from the ZPG case. Skåre and Krogstad (1994) considered a strong APG case near separation. Castillo and George (2001) and Harun et al. (2013) considered both favourable and adverse pressure gradients and compared results of several earlier studies. These are just a few examples. An APG tends to increase turbulence and turbulence production, while a FPG has the opposite effect. Changes in turbulence affect the mean velocity profiles and alter the scaling of the mean velocity and turbulence quantities. Less documented are detailed measurements of the flowfield from which flow structure can be directly observed, as has been done for ZPG cases. Given the changes in statistical quantities that have been observed with different pressure gradients, it is reasonable to assume that the flow structure may change as well. Determining how the LSM respond to pressure gradient changes or if ZPG scaling parameters for them still apply would provide a better understanding of these flows, and could allow better predictions in non-equilibrium cases.

In the present study, a boundary layer on a smooth wall was subject to a strong favourable pressure gradient, followed by a ZPG recovery region, and a strong APG region. In each region, velocity field data were acquired and analysed at multiple streamwise locations to determine how the turbulence structure changes in response to the pressure gradient.

EXPERIMENTS

Experiments were conducted in a water tunnel described in Volino et al. (2007). The test section was 2 m long, 0.2 m wide, and 0.1 m tall at the inlet. The lower wall was a smooth flat plate that served as the test wall and included a trip near the leading edge. The upper wall was comprised of four flat plates that were independently adjusted. The first section was set to provide a ZPG entry region that extended from the trip to x=0.6 m downstream. The second provided a FPG from 0.6 m to 1.1 m. The third section was set for a ZPG recovery from 1.1 m to 1.6 m, and the last section was set for an APG for the rest of the test section. The present paper focuses on a case with inlet freestream velocity U_e=0.5 m/s, and acceleration parameter, $K = (\nu/U_e^2)(dU_e/dx)$=2×10^{-6} in the FPG and -1×10^{-6} in the APG.

Velocity profiles were acquired along the spanwise centreline of the test section at the streamwise locations shown in Table 1 with a two-component LDV. The probe volume diameter was 45 μm. Each profile included about 45 locations ranging from 0.1 mm from the wall to the freestream.

Velocity field data were acquired using PIV at the same locations as the LDV profiles. For each measurement plane, 1000 image pairs were acquired using a CCD camera with a 3320×2496 pixel array. Streamwise-wall normal (x-y) planes were acquired at the spanwise centreline of the test section.

Streamwise-spanwise (x-z) planes were acquired at y/δ=0.15 and 0.4, where δ is the 99% boundary layer thickness.

RESULTS

Mean streamwise velocity profiles are shown in Fig. 1. Also shown for comparison are ZPG profiles from the DNS of Jimenez et al. (2010) at Re_τ close to those of the present profiles. In the FPG region, the wake is strongly suppressed, and the profiles rise above the flat plate law of the wall, in agreement with results from the literature (e.g. Spalart, 1986). Table 1 shows that the boundary layer thickness decreases due to the acceleration. In the ZPG recovery, there is a return to the law of the wall, and growth of the wake resumes, resulting in good agreement with the DNS. In the APG region the growth of the boundary layer and wake are rapid.

The streamwise component of the Reynolds stress, u'^2, exhibits the expected inner and outer peak, as shown in inner coordinates in Fig. 3. The inner peak remains nearly unchanged through the FPG and ZPG recovery, followed by some growth in the APG region. The outer peak is suppressed by the FPG, and then returns rapidly in the ZPG recovery. By the end of the recovery, the profiles agree with the DNS results at the same Re_τ. The outer peak grows rapidly in the APG region. Using the mixed scaling of DeGraff and Eaton (2000), in which u'^2 is normalized using the product $u_\tau U_e$, the inner peak exhibits a small (roughly 10%) rise in the FPG and corresponding drop in the recovery, but collapses better in the APG, showing a small (~5%) reduction below the ZPG value. The outer peak has the same clear trends regardless of scaling.

The wall normal component of the Reynolds stress, v'^2 (not shown), has the same behaviour as the outer peak in u'^2, as does the Reynolds shear stress, $-u'v'$, shown in Fig. 3. In Figs. 2 and 3, note the collapse of the peaks at stations 5 and 6 at the end of the FPG, as the sink flow appears to reach equilibrium, the rapid rise between stations 6 and 7 at the start of the ZPG recovery, the agreement with the ZPG DNS at Stations 8 and 9, and the rapid growth in the APG region. Much of the APG growth in the outer peak is due to the decline in the friction velocity, u_τ, as opposed to an increase in the dimensional magnitude of the turbulence. If the profiles at stations 10-12 were all normalized using either u_τ or U_e at the beginning of the APG region, as suggested by Aubertine and Eaton (2005), the profiles of Figs. 2c and 3c would show good collapse for y^+>150. For y^+<150, this scaling also collapses the v'^2 data, but results in a drop in u'^2 and $-u'v'$ below the ZPG results.

The FPG causes a straining of the turbulence and subsequent reduction in all of the Reynolds stresses. Away from the wall, this results in the suppression of the outer peak. The rising freestream velocity also results in higher dimensional shear in the mean velocity, and this effect is strongest in the near wall region where the mean velocity gradient is highest. This causes u_τ to rise, which also contributes to the drop in the outer peak. Another effect of the higher near wall shear is that turbulent fluctuations across this shear are amplified in the u'^2 component of the Reynolds shear. The net result near the wall is that u'^2 and u_τ^2 scale with each other, leaving the inner peak largely unchanged. The APG has limited effect on the dimensional turbulence in the outer part of the boundary layer, so as u_τ drops, the outer peaks rises. Near the wall, the reduced mean shear results in a reduction of the dimensional Reynolds stresses, particularly those involving the u' component. The friction velocity drops faster, however, resulting in the rising inner peak in Figs. 2c.

Table 1. Boundary layer parameters.

St.	x [m]	K $\times 10^6$	U_e [m/s]	u_τ [m/s]	Re_θ	Re_τ	δ [mm]
1	0.59	0	0.49	0.0239	721	304	12.2
2	0.68	2	0.54	0.0266	668	303	11.5
3	0.77	2	0.57	0.0281	669	360	12.5
4	0.85	2	0.64	0.0320	626	356	11.3
5	0.94	2	0.72	0.0350	611	393	10.9
6	1.06	2	0.97	0.0475	607	448	9.2
7	1.27	0	0.98	0.0440	981	466	10.3
8	1.44	0	0.97	0.0435	1381	559	12.4
9	1.56	0	0.96	0.0404	1855	647	15.7
10	1.67	-1	0.90	0.0340	2294	644	18.4
11	1.74	-1	0.85	0.0290	2765	641	21.7
12	1.81	-1	0.81	0.0248	3291	651	25.7

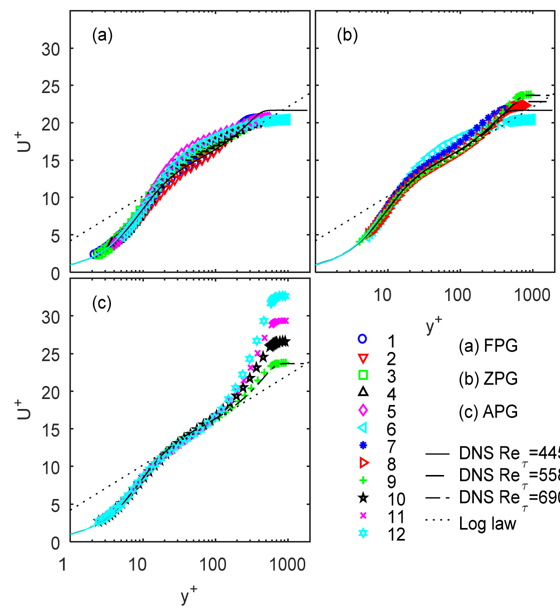

Figure 1. Mean velocity profiles, station number from Table 1.

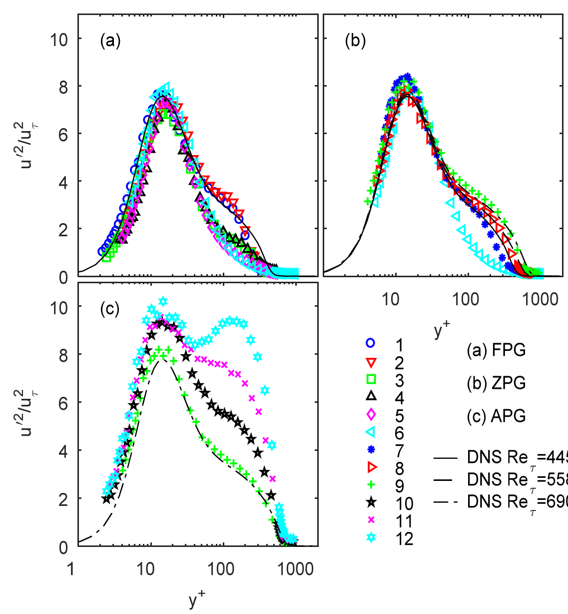

Figure 2. Streamwise Reynolds normal stress profiles.

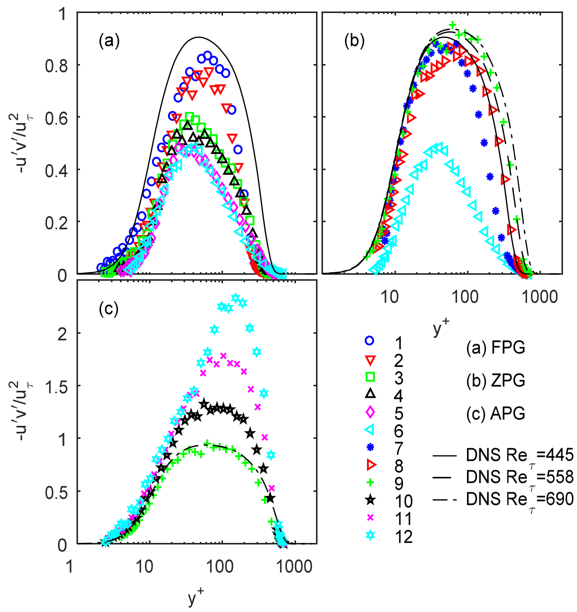

Figure 3. Reynolds shear stress profiles.

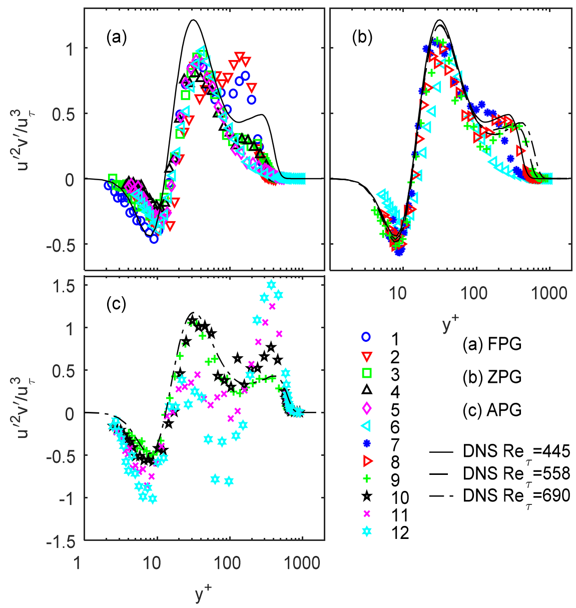

Figure 4. Triple product, u'^2v', profiles.

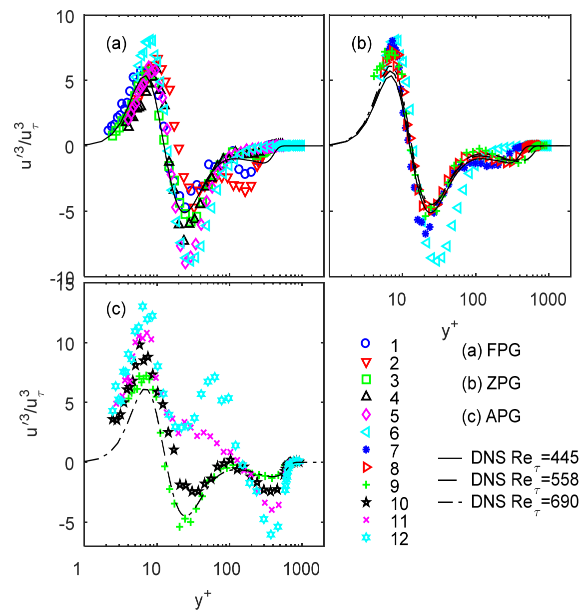

Figure 5. Triple product, u'^3, profiles.

Figure 4 shows profiles of u'^2v'/u_τ^3, which can be considered the wall normal transport term for u'^2. In the FPG region, turbulence from the near wall peak in Fig. 2a is transported toward the wall, resulting in the negative peak at y^+=10 in Fig. 4a. Turbulence from the inner peak is also transported away from the wall, resulting in the positive peak at y^+=30 in Fig. 4a. Turbulence from the outer peak of Fig. 2a is transported away from the wall and produces the outer peak of Fig. 4a at y^+≈250. Presumably, there is also transport from the outer u'^2 peak toward the wall, but this effect on u'^2v' is overwhelmed by the effect of the larger inner peak. Since the FPG has little effect on the inner peak of Fig. 2a and b, there is correspondingly little change in the inner two peaks of Fig. 4. The suppression and recovery of the outer peak in Fig. 4a and b corresponds to the response of the outer peak in Fig. 2 to the FPG. The APG causes significant change in the profiles of Fig. 4c. The rising inner peak in Fig. 2c causes an increase in magnitude of the negative inner peak of Fig. 4. The rising outer peak in u'^2 has a larger effect. Transport toward the wall from this peak drives down the middle peak in Fig. 4c and creates a new negative peak. Transport away from the wall causes the outer peak in u'^2v' to increase in magnitude by a factor of 3.

The primary motions causing the turbulent transport are expected, in terms of quadrant analysis, to be bursts and sweeps (Q2 and Q4 events). Figure 5 shows this for the wall normal transport of u'^2 with profiles of u'^3. The peaks in Fig. 5 correspond to and have the same behaviour as those in Fig. 4, but are of larger magnitude and opposite sign, indicating that the transport of u'^2 toward and away from the wall is indeed caused by Q2 and Q4 events respectively.

Following the same arguments, the triple product $-u'v'^2$ could be associated with the wall normal transport of the Reynolds shear stress, or with the streamwise fluctuations corresponding to the wall normal transport of v'^2. The profiles in Fig. 6 may include elements of both. A motion transporting $-u'v'$ toward the wall would cause the negative peak near y^+=10 in Fig. 6. A Q4 even carrying v'^2 toward the wall would produce the same result. Motions in the opposite direction would produce the positive peak away from the wall. As in the figures above, the fall and rise of the quantities being transported caused by the FPG and APG result in the response seen in Fig. 6. The double positive peak in Fig. 6 could be due to the separate effects of the transport of $-u'v'$ and v'^2, which do not have their peaks in exactly the same locations. One could similarly argue that $u'v'^2$ of Fig. 4 may include the effects of the transport of both $-u'v'$ and u'^2, although at least for the inner peak, it is the u'^2 effect that dominates.

The underlying flow structure that results in the changes in the profiles of Figs. 1-6 was investigated using quadrant analysis. As expected Q2 and Q4 dominate at all streamwise locations. Qualitatively, the contribution to $-u'v'$ from each individual quadrant responds to the pressure gradient in the same way as the full $-u'v'$ of Fig. 3. The relative importance of different motions changes in response to the pressure gradient, however, particular the importance of bursts compared to

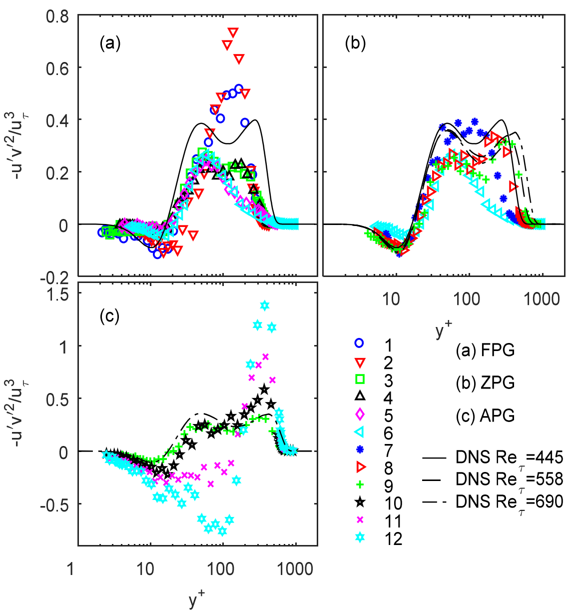

Figure 6. Triple product, $u'v'^2$, profiles.

sweeps. Figure 7 shows the ratio of the contribution of Q2 and Q4 events to the Reynolds shear stress at representative streamwise stations (end of entry ZPG, end of FPG, end of ZPG recovery, end of APG). Very near the wall, the data from all stations collapse and since there is little fluid even closer to the wall from which bursts can originate, sweeps contribute more, and the ratio of Q2 to Q4 is low. Near the edge of the boundary layer, the opposite is true. The sweep contribution from the freestream is low, so Q2/Q4 is high. In the ZPG region, the ratio of Q2 to Q4 contributions plateaus at about 1.2 in the middle of the boundary layer. The FPG causes a rise to about 1.7. The APG has the opposite effect, causing the plateau to drop to 0.9. The quadrant results are consistent with the profiles presented above. The suppression of the turbulence in the outer region caused by the FPG appears to result in fewer significant sweep events relative to bursts. The reduction of the near wall shear caused by the APG results in fewer bursts relative to sweeps.

To further illustrate the flow structure, two-point spatial correlation in the *x-y* plane are shown in Fig. 8. The correlations are centred at y/δ=0.4 and have been averaged in the streamwise direction and time averaged over the 1000 image pairs. The behaviour at y/δ=0.4 is representative of other locations in the boundary layer. The columns in Fig. 8 are for the same stations shown in Fig. 7. From top to bottom the rows show the auto correlation of streamwise fluctuating velocity, R_{uu}; the auto correlation of the wall-normal fluctuating velocity, R_{vv}; the cross correlation R_{-uv}; the cross correlation of the two-dimensional signed swirl strength, λ, and the streamwise velocity fluctuations, $R_{\lambda u}$; and the cross correlation $R_{\lambda v}$. The swirl strength is useful for identifying vortices, and is the part of the vorticity attributable to rotation as opposed to shear. It is used here as in Volino et al. (2007) and described in Hutchins et al. (2005). The ZPG results agree with previous findings in the literature (e.g. Volino et al., 2007). The R_{uu} contours suggest the shape of a hairpin packet. In the FPG region, they are elongated in the streamwise direction. This is quantified in Fig. 9, which shows a cut through the self-correlation point. The inclination angle of the contours, θ, and the streamwise, L_x, and wall normal, L_y, extent of the R_{uu}=0.5 contour, as described in Volino et

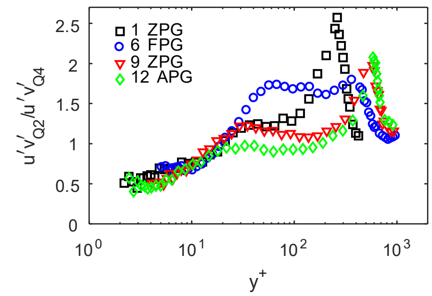

Figure 7. Ratio of Q2 to Q4 contribution to $-u'v'$.

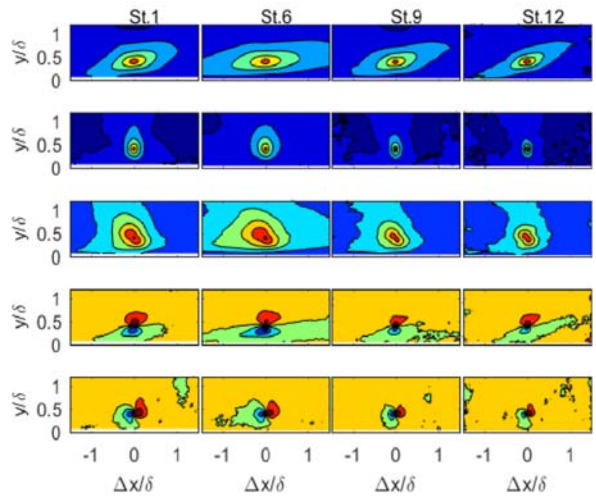

Figure 8. Correlation contours in *x-y* plane centred at y/δ=0.4. Quantity and linear contour range from blue to red by row: Top R_{uu}, -0.1 to 1; 2nd R_{vv}, -0.1 to 1; 3rd R_{-uv}, -0.15 to 0.45; 4th $R_{\lambda u}$, -0.2 to 0.08; Bottom $R_{\lambda v}$, -0.2 to 0.08.

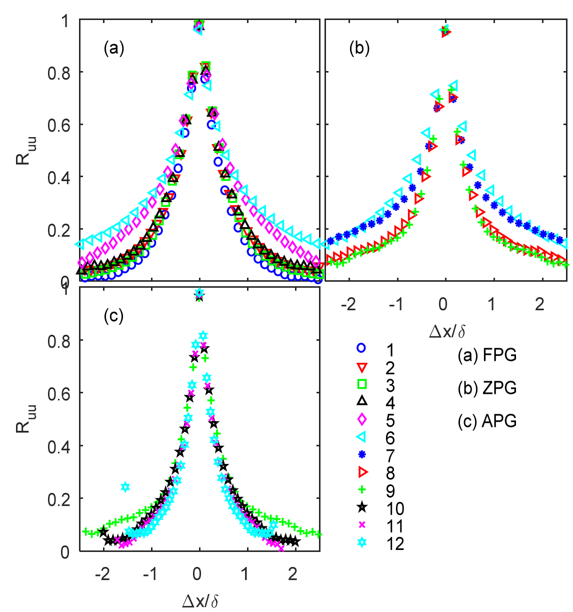

Figure 9. Streamwise cut through R_{uu} contour at y/δ=0.4.

al. (2007) are shown in Fig. 10. These values remain approximately constant across the middle of the boundary layer, and those shown are averages for R_{uu} centred between y/δ=0.3

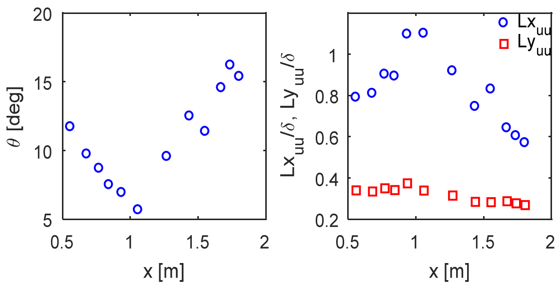

Figure 10. Inclination angle of R_{uu} contours (left), and streamwise and wall-normal extent of R_{uu}=0.5 contour (right).

and 0.7. As the flow proceeds through the FPG region, L_x/δ increases by about 35%, and θ decrease from about 12° to 6°. Both return to their original values in the ZPG recovery. In the APG, θ increases to about 15°. The changes in L_y follow the same trend as in L_x, but are much smaller.

The trends in R_{uu} also apply to the other quantities in Fig. 8, but the extent of the correlations involving v' are lower in the streamwise direction. The $R_{\lambda u}$ correlation shows that a vortex at the centre of the correlation is more correlated with events closer to the wall than with the outer part of the boundary layer. This is particularly true in the FPG region, where the streamwise length of the correlation is extended. The suppression of outer region turbulence caused by the FPG results in less of an extension of the large flow structures into this region, reducing the inclination angle of R_{uu} and $R_{\lambda u}$. The reduction in the effect of sweeps from the outer region may result in less disruption of the inner region flow, resulting in longer streamwise correlation lengths.

Linear stochastic estimation (LSE) provides another means of examining the flow structure, and is shown in Fig. 11 for the streamwise wall-normal planes of the streamwise stations of Fig. 7. The processing used is described in Volino et al. (2009). LSE shows the average velocity field associated with a particular event in the flow, in this case a clockwise swirl at y/δ=0.4. Such an event is associated with the head of a hairpin vortex. The correlated region in the figure is characterized by organized appearing vectors, while the vectors outside this region appear random. Note that all vector lengths are the same and indicate direction, not magnitude. The results at the ZPG stations agree with those in Volino et al. (2009). Included is a crease extending upward and to the right through the centre of the correlation. Along this crease appear patterns suggesting vortices that may be associated with a hairpin packet. The FPG reduces the inclination angle of the crease and extends the correlated region near the wall to beyond the field of view, in agreement with the results of Fig. 8. In the APG the correlated region is slightly smaller, but similar to the ZPG. The boundary layer thickness grows in the APG region, as shown in Table 1, so as δ increases, the size of the structures increase approximately proportionally.

Figure 12 shows an example from the x-z plane, with the cross correlation of streamwise and spanwise (w') fluctuations at distances of y/δ=0.15 and 0.4 from the wall. Results were averaged in the streamwise and spanwise directions and over 1000 image pairs. The signs and shapes of the contours are consistent with the flow induced by the legs of hairpin vortices. The structures have different shapes at the two y locations and are smaller near the wall, but the trend with pressure gradient is the same at both locations. During the FPG, at y/δ=0.40 the dimensionless size of the structure increases by about a factor of 2 in both the streamwise and spanwise directions, then quickly

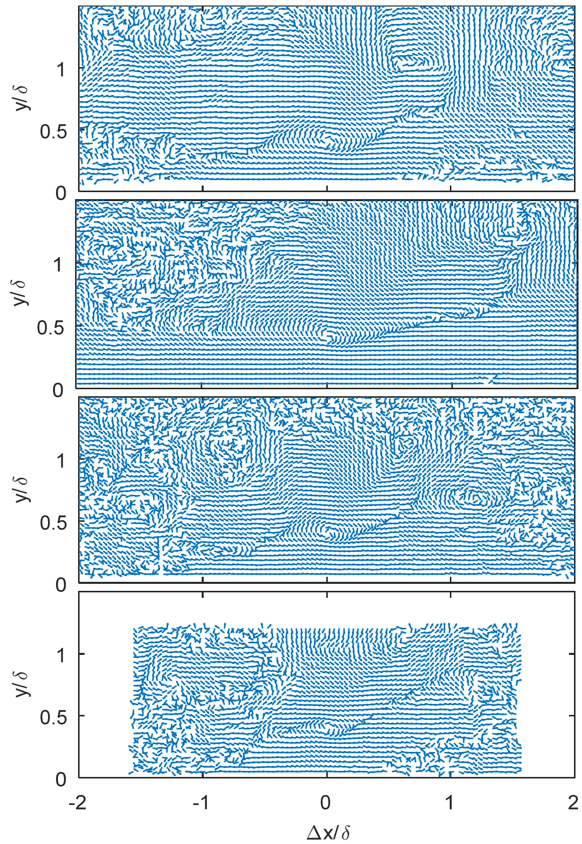

Figure 11. LSE conditioned on swirl event in x-y plane at y/δ=0.4 at (top to bottom) stations 1, 6, 9, and 12.

returns to the original size in the ZPG recovery. The change is less but still significant at y/δ=0.15. There is little change in the APG region, as the size of the structure scales with δ.

Figure 13 shows the $R_{\lambda u}$ correlation in the same format. This correlation, along with R_{uu}, exhibits long streamwise streaks of alternating sign across the field of view. The extent of the correlation, albeit weak, is also apparent across the visible span. As with R_{uw}, the width of the streaks increases with the FPG, recovers quickly in the ZPG region, and changes little in the APG. Figure 13 suggests that the structures are associated with vortices, and Fig. 14 supports this using LSE conditioned on the appearance of a vortex in the same plane. The vortex at the centre of the field is clearly visible, as are two vortices of opposite sign at $\Delta z/\delta\approx\pm0.4$. Another pair, rotating in the same direction as the central vortex is present at $\Delta z/\delta\approx\pm0.8$. Also visible are streamwise streaks of positive and negative u′. The spacing of the vortices indicate the average spacing of the legs of a hairpin, and the steaks show the flow induced within a hairpin packet. Figure 15 shows the average spanwise spacing of the vortices as a function of streamwise location. In agreement with results above, the spacing increases in the FPG region and decreases in the ZPG recovery and APG.

CONCLUSIONS

Pressure gradients were shown to have a significant effect on the structure of turbulent boundary layers. A FPG reduces all components of the turbulence in the outer part of the boundary

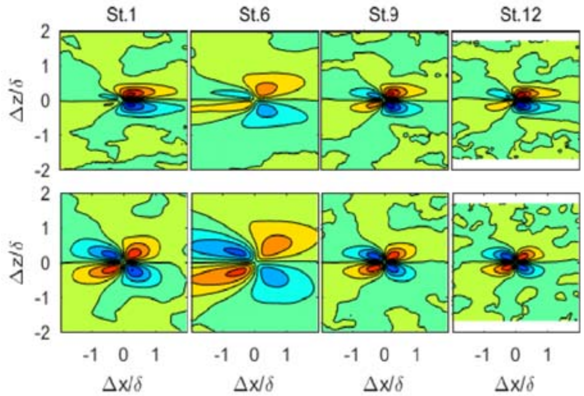

Figure 12. R_{uw} contours in *x-z* plane for stations 1, 6, 9, and 12 at y/δ=0.15(top) and y/δ=0.4 (bottom).

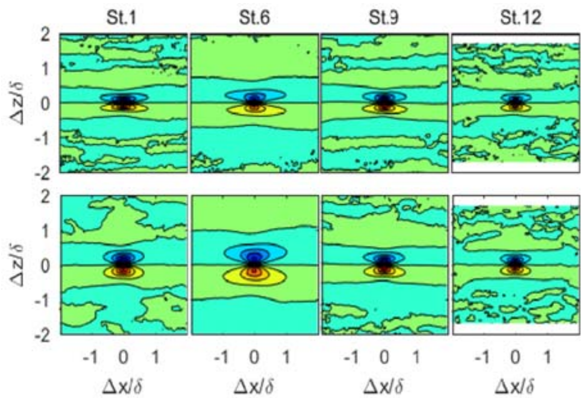

Figure 13. $R_{\lambda u}$ contours in *x-z* plane for stations 1, 6, 9, and 12 at y/δ=0.15(top) and y/δ=0.4 (bottom).

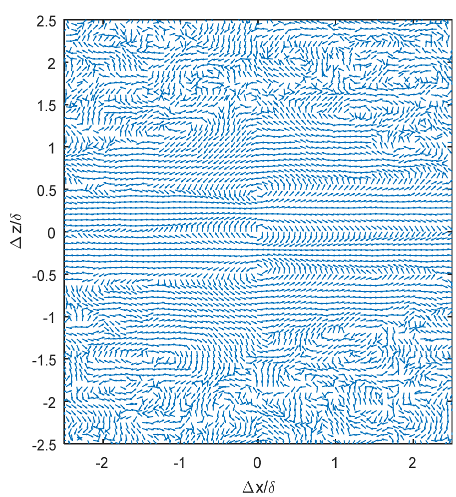

Figure 14. LSE conditioned on swirl in *x-z* plane at y/δ=0.4.

layer along with the subsequent transfer of that turbulence. This reduces the effect of sweep events towards the wall, increases length scales, particularly in the streamwise and spanwise directions, and reduces the inclination angle of the large structures. Recovery from a FPG to a ZPG appears to be rapid. An APG reduces near wall shear and the significance of burst events, with a less pronounced effect on the size of structures when scaled on the boundary layer thickness.

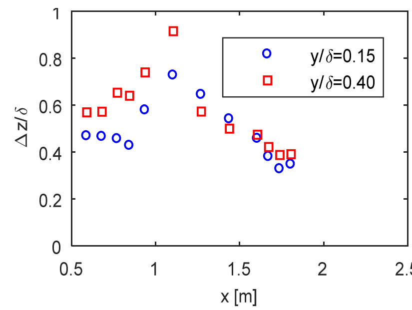

Figure 18. Spanwise distance between vortices detected by LSE in *x-z* planes at y/δ=0.15 and 0.40.

ACKKNOWLEDGMENTS

The support of the U.S. Office of Naval Research, and the assistance of the U.S. Naval Academy Hydromechanics Laboratory and Project Support Branch are greatly appreciated.

REFERENCES

Adrian, R. J., Meinhart, C. D. and Tomkins, C. D., 2000, "Vortex organization in the outer region of the turbulent boundary layer," *Journal of Fluid Mechanics*, Vol. 422, pp. 1-54.

Aubertine, C. D. and Eaton, J. K., 2005, "Turbulence development in a non-equilibrium turbulent boundary layer with mild adverse pressure gradient," *Journal of Fluid Mechanics*, Vol. 532, pp. 345-364.

Castillo, L. and George, W. K., 2001, "Similarity Analysis for Turbulent Boundary Layer with Pressure Gradient: Outer Flow," *AIAA Journal*, Vol. 39, pp. 41-47.

DeGraff, D. B. and Eaton, J. K., 2000, "Reynolds-number scaling of the flat-plate turbulent boundary layer," *Journal of Fluid Mechanics*, Vol. 422, pp. 319-346.

Ganapathisubramani, B., Longmire, E. K. and Marusic, I., 2003, "Characteristics of vortex packets in turbulent boundary layers," *Journal of Fluid Mechanics*, Vol. 478, pp. 35-46.

Hambleton, W. T., Hutchins, N. and Marusic, I., 2006, "Simultaneous orthogonal-plane particle image velocimetry measurements in a turbulent boundary layer," *Journal of Fluid Mechanics*, Vol. 560, pp. 53-64.

Harun, Z., Monty, J. P., Mathis, R. and Marusic, I., 2013, "Pressure gradient effects on the large-scale structure of turbulent boundary layers," *Journal of Fluid Mechanics*, Vol. 715, pp. 477-498.

Hutchins, N., Hambleton, W. T. and Marusic, I., 2005, "Inclined cross-stream stereo particle image velocimetry measurements in turbulent boundary layers," *Journal of Fluid Mechanics*, Vol. 541, pp. 21-54.

Jimenez, J., Hoyas, S., Simens, M. P., and Mizuno, Y., 2010, "Turbulent boundary layers and channels at moderate Reynolds numbers," *Journal of Fluid Mechanics*, Vol. 657, pp. 335-360.

Skåre, P. E. and Krogstad, P.-Å., 1994, "A turbulent equilibrium boundary layer near separation," *Journal of Fluid Mechanics*, Vol. 532, pp. 319-348.

Spalart, P. R., 1986, "Numerical study of sink-flow boundary layers," *Journal of Fluid Mechanics*, Vol. 172, pp. 307-328.

Volino, R. J., Schultz, M. P. and Flack, K. A., 2007, "Turbulence structure in rough- and smooth-wall boundary layers," *Journal of Fluid Mechanics*, Vol. 592, pp. 263-293.

Volino, R. J., Schultz, M. P. and Flack, K. A., 2009, "Turbulence structure in a boundary layer with two-dimensional roughness," *Journal of Fluid Mechanics*, Vol. 635, pp. 75-101.